and, from differentiating Eq. (6) using Eq. (8),

$$2\Delta v_k\,(\partial \Delta v_k/\partial e) = 2v_k\,(\partial v_k/\partial e) = 2e\mu/p \tag{10}$$

Thus

$$\partial \Delta v_T/\partial e = (e\mu/p)(\Delta v_1^{-1} + \Delta v_2^{-1}) > 0 \tag{11}$$

The fact that the partial derivative of the characteristic velocity with respect to the eccentricity is positive means that at any point (p,e) in the interior of the feasible region the characteristic velocity can be decreased by decreasing the value of e while holding the value of p constant. This means that the minimum characteristic velocity will always lie on the cross-hatched boundary of the feasible region given by the union of $r_a = r_2$ and $r_p = r_1$ in Fig. 1.

What will be demonstrated is that when the characteristic velocity is constrained to the boundary, its derivative with respect to e remains positive. Thus the optimal solution lies at the minimum value of e on the boundary, i.e., at point H in Fig. 1, which represents the Hohmann transfer.

To do this, the expression for the characteristic velocity is constrained to the boundary by substituting for the value of p along each portion of the boundary, namely $p = r_2(1-e)$ on the left part ($r_a = r_2$) and $p = r_1(1+e)$ on the right part ($r_p = r_1$). Thus the characteristic velocity becomes a function of the single variable e. Letting $\Delta\tilde{v}$ denote the velocity change constrained to the boundary, Eq. (6) becomes for the left part

$$(\Delta\tilde{v})^2 = \mu\left[\frac{2}{r} + \frac{e^2-1}{r_2(1-e)}\right] + \frac{\mu}{r} - 2\left(\frac{\mu}{r}\right)^{1/2}\frac{[\mu r_2(1-e)]^{1/2}}{r} \tag{12}$$

Differentiating with respect to the single variable e and recalling that $R = r_2/r_1 > 1$ and $0 < e < 1$,

$$2\Delta\tilde{v}_1\frac{d\Delta\tilde{v}_1}{de} = \frac{\mu}{r_2}\left[R^{3/2}\frac{1}{(1-e)^{1/2}} - 1\right] > 0 \tag{13}$$

and

$$2\Delta\tilde{v}_2\frac{d\Delta\tilde{v}_2}{de} = \frac{\mu}{r_2}\left[\frac{1}{(1-e)^{1/2}} - 1\right] > 0 \tag{14}$$

and thus, similar to Eq. (11), $d\Delta\tilde{v}_T/de > 0$ on the left portion of the boundary.

Similarly, on the right portion of the boundary,

$$(\Delta\tilde{v})^2 = \mu\left[\frac{2}{r} + \frac{e^2-1}{r_1(1+e)}\right] + \frac{\mu}{r} - 2\left(\frac{\mu}{r}\right)^{1/2}\frac{[\mu r_1(1+e)]^{1/2}}{r} \tag{15}$$

Differentiating, one obtains

$$2\Delta\tilde{v}_1\frac{d\Delta\tilde{v}_1}{de} = \frac{\mu}{r_1}\left[1 - \frac{1}{(1+e)^{1/2}}\right] > 0 \tag{16}$$

and

$$2\Delta\tilde{v}_2\frac{d\Delta\tilde{v}_2}{de} = \frac{\mu}{r_1}\left[1 - \frac{1}{R^{3/2}(1+e)^{1/2}}\right] > 0 \tag{17}$$

and thus, $d\Delta\tilde{v}_T/de > 0$ on the right portion of the boundary also. Because the derivative of $\Delta\tilde{v}_T$ with respect to the eccentricity is positive at all points on the boundary, it follows that the optimal solution lies at the point of minimum eccentricity on the boundary, namely at point H in Fig. 1, representing the Hohmann transfer. This proves the global optimality of the Hohmann transfer among two-impulse transfers.

As mentioned by Edelbaum,[8] for values of R greater than approximately 11.94 (printed as 11.24 in Ref. 8 due to a typographical error), the Hohmann transfer is no longer the global optimal impulsive transfer. A three-impulse bielliptic transfer can always be found that has a lower cost, if the midcourse impulse occurs sufficiently far outside the outer terminal orbit. For R greater than approximately 15.58, any bielliptic transfer that has its midcourse impulse outside the outer terminal orbit has a lower cost than the Hohmann transfer.[2,6,8] The major disadvantage of the bielliptic transfer is that the transfer time is more than twice the Hohmann transfer time, while the cost saving in the coplanar case is modest. In the noncoplanar case, the bielliptic transfer provides significant cost savings[8] because the required plane change can be accomplished at larger radius and therefore lower velocity.

There exists no optimal bielliptic transfer, but the infimum of the bielliptic transfers is the biparabolic transfer, which is the limiting case of the bielliptic transfer as the midcourse impulse location tends to infinity. However, for all values of R, the Hohmann transfer is the globally optimal two-impulse transfer, based on the proof given above.

Concluding Remarks

The case of two-impulse transfer between coplanar circular orbits is investigated. By using the familiar orbital elements, eccentricity e and parameter (semilatus rectum) p, the global optimality of the Hohmann transfer among the class of two-impulse transfers is proved using ordinary calculus. The proof presented is simpler than existing proofs in the literature.

Acknowledgment

This research was supported by NASA Research Grant NAG 3-1138 administered by the Systems Analysis Branch of the NASA Lewis Research Center.

References

[1]Hohmann, W., *Die Erreichbarkeit der Himmelskörper,* Oldenbourg, Munich, 1925; also, NASA Technical Translation F-44, 1960.

[2]Lawden, D. F., *Optimal Trajectories for Space Navigation,* Butterworths, London, 1963, Chap. 6.

[3]Barrar, R. B., "An Analytic Proof that the Hohmann-Type Transfer is the True Minimum Two-Impulse Transfer," *Astronautica Acta,* Vol. 9, No. 1, 1963, pp. 1-11.

[4]Hazelrigg, G. A., Jr., "The Use of Green's Theorem to Find Globally Optimal Solutions to a Class of Impulsive Transfers," American Astronomical Society, AAS Paper 68-092, Sept. 1968.

[5]Marec, J. P., *Optimal Space Trajectories,* Elsevier, Amsterdam, 1979, Chap. 2, pp. 21-27.

[6]Battin, R. H., *An Introduction to the Mathematics and Methods of Astrodynamics,* AIAA Education Series, AIAA, New York, 1987, pp. 529-530.

[7]Palmore, J. I., "An Elementary Proof of the Optimality of Hohmann Transfers," *Journal of Guidance, Control, and Dynamics,* Vol. 7, No. 5, 1984, pp. 629-630.

[8]Edelbaum, T. N., "How Many Impulses?" *Astronautics and Aeronautics,* Nov. 1967, pp. 64-69.

Symptom of Payload-Induced Flight Instability

Charles H. Murphy*
U.S. Army Ballistic Research Laboratory, Aberdeen Proving Ground, Maryland 21005

Introduction

THE angular motion of a projectile in flight can usually be represented as the sum of two coning motions. The stabil-

Received May 16, 1991; revision received Sept. 26, 1991; accepted for publication Sept. 27, 1991. This paper is declared a work of the U.S. Government and is not subject to copyright protection in the United States.

*Chief, Launch and Flight Division, SLCBR-LF. Fellow AIAA.

ity of a general motion can then be determined by considering the stability of each coning motion separately. For this analysis, an aeroballistic coning axis system with unit vectors $\hat{e}_{xc}$, $\hat{e}_{yc}$, and $\hat{e}_{zc}$ is customary. The $\hat{e}_{xc}$ vector is aligned along the projectile's axis of symmetry; the $\hat{e}_{yc}$ vector is in the plane containing the axis of symmetry and the velocity vector and points toward the velocity vector. For constant-amplitude coning motion of amplitude α_c and frequency $\dot{\phi}_c$, the angular velocity of the coordinate system is

$$\Omega = \dot{\phi}_c(\hat{e}_{xc} \cos \alpha_c + \hat{e}_{yc} \sin \alpha_c) \quad (1)$$

The aerodynamic moment M_a can be expressed in the coning coordinate system as (M_{ax}, M_{ay}, M_{az}). M_{ax} represents the spin moment and is usually described quantitatively by the dimensionless coefficient C_l. M_{az} represents an in-plane moment (a moment causing a motion in the plane of the cone angle); it is related primarily to the static moment coefficient C_{M_α} and controls the frequency of the coning motion.[1] Finally, M_{ay} represents a side moment; it is a combination of the damping-in-pitch and Magnus moment coefficients and controls the growth or decay of the coning motion.

If a projectile has a moving payload, solid or liquid, the moment exerted by this payload can be expressed in coning coordinates as (M_{px}, M_{py}, M_{pz}). The side moment component M_{py} can cause spectacular instabilities. When these instabilities occur, a rapid despin is observed; hence, a relation between the moving payload's spin moment and its side moment has long been suspected. This correlation between spin and side moment is used as a diagnostic for payload-induced instability.

In this Note, we will review the experimental observations and theories that deal with this relation for a variety of moving components. We will then derive a very simple relation that applies to all moving payloads in steady-state motion, thus validating the diagnostic tool.

Moving Rigid Payload

In 1955, an 8-in. shell, the T317, showed significant range losses and very large spin decays.[2] This shell had several rings held on a central column but free to move within small but nonzero clearances. The actual spin histories of several T317s are given in Ref. 2 and are repeated as Fig. 1. This figure also gives the spin history for three T347s. The T347 shell has the same external shape, mass, and moments of inertia as the T317 but no movable internal components. In all observed cases, the T317 had a greater spin loss and flew to a lesser range. The relative decrements between the range of each T317 shell and the average range of the T347s are given in the figure. We see that a spin loss of almost 70 Hz was observed for a projectile that flew 11% short of its proper range.

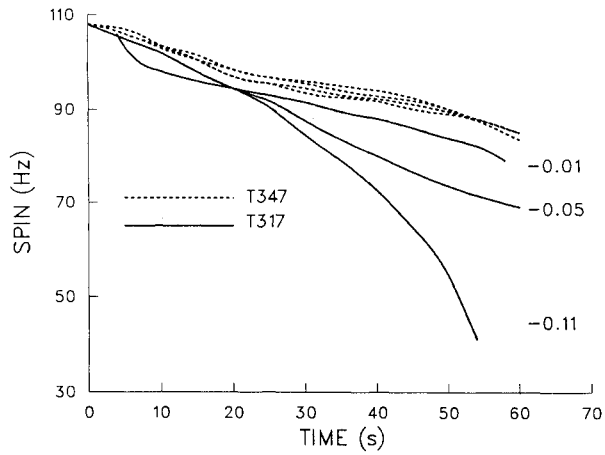

Fig. 1 Measured spin histories of T317.

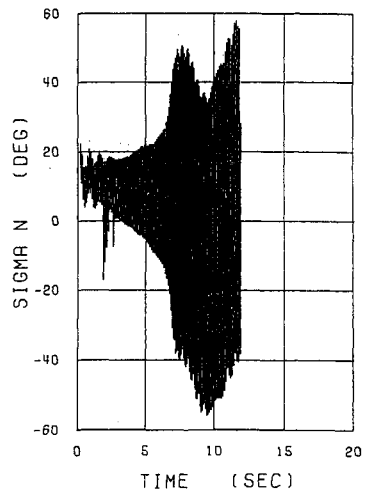

Fig. 2 Sun angle history of unstable liquid-filled shell.

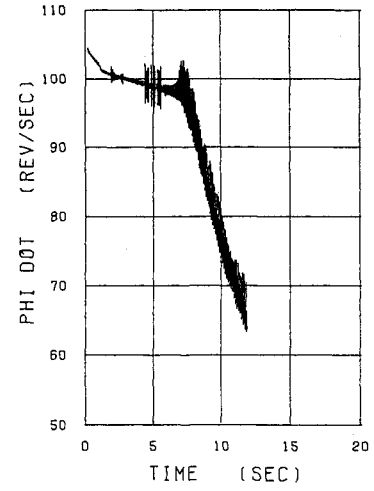

Fig. 3 Spin history of unstable liquid-filled shell.

Several authors[3-5] developed steady-state payload motion theories to explain this misbehavior. Reference 5 considered two types of motion: 1) a circular motion of radius ϵ of the payload component center of mass about the projectile's axis of symmetry, and 2) a coning motion of angle γ of the spin axis of the payload component about the projectile's axis of symmetry. Both motions were assumed to be at the projectile's coning frequency $\dot{\phi}_c$ and lagging the projectile coning motion by a phase angle ϕ_a. Under these assumptions, the side moment exerted by the internal component was shown to be

$$M_{py} = A\dot{\phi}_c \sin \phi_a \quad (2)$$

where A is a function of certain physical characteristics of the internal component.

More importantly, the roll moment induced by the payload component was shown to be

$$M_{px} = -M_{py} \sin \alpha_c \quad (3)$$

Liquid Payloads

Liquid payloads have been known to cause very spectacular instabilities. Flight measurements in 1974 of unstable projectiles with spinning liquid payloads showed a most remarkable result.[6] Very large decreases in projectile spin were observed for unstable projectiles performing large-amplitude coning motion.

Figures 2 and 3 are yawsonde records for a liquid-filled shell fired at a transonic muzzle velocity. The oscillating sun angle

σ_n indicates a coning motion in excess of 30 deg after 8 s of flight. At this time, the slope of the Euler spin $\dot{\phi}$ changes by a factor of 10. Thus, projectiles fully filled with liquid show the same spin-down behavior as projectiles with moving rigid payloads. Indeed, this large despin moment occurring for payload-induced instability was suggested by Miller[7] as a design tool, a technique justified by flight tests.[8]

The first theoretical relation between side moment and roll moment for liquid payloads in a cylindrical container was given in Ref. 9. This reference assumed that the steady-state motion of a liquid could be approximated by a linearized Navier-Stokes equation and then showed (after considerable algebra) that Eq. (3) was valid for a liquid payload. Later, Rosenblat et al.[10] showed that linearization of the Navier-Stokes equation was unnecessary. After three pages of much simpler algebra, Ref. 10 showed that any liquid in a fully filled cylindrical cavity (provided the liquid satisfies the continuity equation and is in steady-state motion) has the following relationship between its side moment and its roll moment:

$$M_{px} = -M_{py} \tan \alpha_c \tag{4}$$

Note that the linear versions of Eqs. (3) and (4) are the same but Eq. (4), which is based on the nonlinear Navier-Stokes equations, is the more accurate nonlinear version.

General Moving Payload Moment Relation

The occurrence of Eq. (4) in so many moving payload theories suggests the possibility that some simple general proof of this relation should exist for all possible moving payloads in steady-state motion. Indeed, such a proof was developed in Ref. 11 by differentiating the angular momentum of the moving payload.

The moment exerted by the moving payload is the negative of the derivative of the payload's angular momentum:

$$\boldsymbol{M}_p = -(\dot{L}_1 \hat{e}_{xc} + \dot{L}_2 \hat{e}_{yc} + \dot{L}_3 \hat{e}_{zc} + \boldsymbol{\Omega} \times \boldsymbol{L}) \tag{5}$$

where (L_1, L_2, L_3) are the coning system components of the payload angular momentum vector.

For steady-state coning motion, $\dot{L}_j = 0$ and, hence,

$$\boldsymbol{M}_p = \dot{\phi}_c \left[-L_3 \sin \alpha_c \hat{e}_{xc} + L_3 \cos \alpha_c \hat{e}_{yc} + (L_1 \sin \alpha_c - L_2 \cos \alpha_c) \hat{e}_{zc} \right] \tag{6}$$

so that

$$M_{px} = -M_{py} \tan \alpha_c \tag{7}$$

Conclusions

The presence of a payload-induced side moment can always be identified by the roll moment for large coning motion. Even more importantly, the payload side moment can be measured in ground tests by measurement of the spin moment exerted by a payload doing a forced coning motion.

References

[1]Murphy, C. H., "Free Flight Motion of Symmetric Missiles," U.S. Army Ballistic Research Laboratory, Aberdeen Proving Ground, MD, Rept. 1216, AD 442757, July 1963.

[2]Karpov, B. G., and Bradley, J. W., "A Study of Causes of Short Ranges of the 8 Inch, T317 Shell," U.S. Army Ballistic Research Laboratory, Aberdeen Proving Ground, MD, Rept. 1049, AD 377548, May 1958.

[3]Chadwick, W. R., "Stability of Spinning Shell (Influence of Elastically Supported Gyroscopic Mass)," unpublished Naval Surface Weapons Center manuscript, Dahlgren, VA, Sept. 1975.

[4]Soper, W. G., "Projective Instability Produced by Internal Friction," *AIAA Journal*, Vol. 16, No. 1, 1978, pp. 8-11.

[5]Murphy, C. H., "Influence of Moving Internal Parts on Angular Motion of Spinning Projectiles," *Journal of Guidance and Control*, Vol. 1, No. 2, 1978, pp. 117-122; see also BRL-MR-2731, AD A037338, Feb. 1977.

[6]D'Amico, W. P., Oskay, V., and Clay, W. H., "Flight Tests of the 155mm XM687 Binary Projectile and Associated Design Modifications Prior to the Nicolet Winter Test 1974-1975," U.S. Army Ballistic Research Laboratory, Aberdeen Proving Ground, MD, MR 2748, AD B019969, May 1977.

[7]Miller, M. C., "Flight Instabilities of Spinning Projectiles Having Nonrigid Payloads," *Journal of Guidance, Control, and Dynamics*, Vol. 5, No. 2, 1982, pp. 151-157.

[8]D'Amico, W. P., and Miller, M. C., "Flight Instability Produced by a Rapidly Spinning, Highly Viscous Liquid," *Journal of Spacecraft and Rockets*, Vol. 16, No. 1, 1976, pp. 62-64.

[9]Murphy, C. H., "Liquid Payload Roll Moment Induced by a Spinning and Coning Projectile," U.S. Army Ballistic Research Laboratory, Aberdeen Proving Ground, MD, ARBRL-TR-02521, AD A133681, Sept. 1983; also, AIAA Paper 83-2142, Aug. 1983.

[10]Rosenblat, S., Gooding, A., and Engleman, M. S., "Finite Element Calculations of Viscoelastic Fluid Flow in a Spinning and Nutating Cylinder," U.S. Army Armament Munitions Chemical Command, Aberdeen Proving Ground, MD, CRDEC-CR-87021, Dec. 1986.

[11]Murphy, C. H., Bradley, J. W., and Mermagen, W. H., Sr., "Side Moment Induced by a Spinning, Coning, Highly Viscous Liquid Payload," U.S. Army Ballistic Research Laboratory, Aberdeen Proving Ground, MD, BRL-TR-3074, AD 218746, Dec. 1989.

Two Variations of Certainty Control

Salvatore Alfano*
U.S. Air Force Academy,
Colorado Springs, Colorado 80840

Introduction

CERTAINTY control[1] enhances interceptor performance by using a terminal guidance law that incorporates the dynamics of the interceptor and target plus the error knowledge of their estimates. This is done by constraining the final estimated state to a spherical inequality based on the projected estimate error. The control law reduces intercept maneuvering when the controls associated with cost do not affect state estimate certainty.[2]

Two variations of certainty control are presented in an attempt to further improve interceptor performance: the first uses a control effectiveness ratio to regulate thrusting times; the second changes the certainty control constraint to an ellipsoidal function based on projected estimate error. Conceptually, the second variation produces a shrinking ellipsoid about the predicted impact point with the surface being a function of estimated error; if the predicted miss is inside or touching the ellipsoid, thrusting is not necessary.

Variational performances in lateral thrusting are examined for a hypervelocity, exoatmospheric, orbital vehicle in the final 30 s of flight while it is attempting to intercept a boosting missile. System modeling and measurement processing are identical to those used in Ref. 1. Target tracking is accomplished with a ranging device and line-of-sight sensors for in-plane and out-of-plane measurements. Noise-corrupted data are processed through an eight-state extended Kalman filter (EKF) with serial updates occurring every 0.1 s. Velocity changes are determined by varying impact conditions using splines to reduce computational burdens and allow a solution that lends itself to deterministic techniques.

Optimum Spacing of Corrective Thrusts

Corrective thrusting in the presence of state estimate errors can be optimally spaced to reduce fuel. A control effectiveness

Received Aug. 5, 1991; revision received Oct. 29, 1991; accepted for publication Nov. 16, 1991.

*Associate Professor, Deputy for Labs and Research, Department of Astronautics. Senior Member AIAA.